Structural Evidence of T Cell Xeno-reactivity in the Absence of Molecular Mimicry

By Rui Zhao,* Douglas J. Loftus,‡ Ettore Appella,‡ and Edward J. Collins*§

*From the *Department of Microbiology and Immunology, University of North Carolina at Chapel Hill, Chapel Hill, North Carolina 27599; and the ‡Laboratory of Cell Biology, National Cancer Institute, National Institutes of Health, Bethesda, Maryland 20892*

Summary

The T cell receptor (TCR), from a xeno-reactive murine cytotoxic T lymphocyte clone AHIII12.2, recognizes murine H-2D^b complexed with peptide p1027 (FAPGVFPYM), as well as human HLA-A2.1 complexed with peptide p1049 (ALWGFFPVL). A commonly proposed model (the molecular mimicry model) used to explain TCR cross-reactivity suggests that the molecular surfaces of the recognized complexes are similar in shape, charge, or both, in spite of the primary sequence differences. To examine the mechanism of xeno-reactivity of AHIII12.2, we have determined the crystal structures of A2/p1049 and D^b/p1027 to 2.5 Å and 2.8 Å resolution, respectively. The crystal structures show that the TCR footprint regions of the two class I complexes are significantly different in shape and charge. We propose that rather than simple molecular mimicry, unpredictable arrays of common and differential contacts on the two class I complexes are used for their recognition by the same TCR.

Key words: major histocompatibility complex • crystallography • xeno-reactivity • transplantation • T cell receptor

The TCR, expressed on the surface of CD8$^+$ CTL, recognizes specific class I MHC/peptide complexes on APC. The result of the recognition is typically lysis of the APC. The mature class I molecule is a ternary complex containing a glycoprotein heavy chain, a noncovalently associated light chain β_2-microglobulin (β_2m),[1] and a small antigenic peptide (typically 8–10 residues). Crystal structures of class I/peptide complexes reveal that the peptide-binding region of class I is a cleft formed by two α helices in the α1 and α2 domains of the heavy chain (for review see reference 1). Each specific class I molecule binds a large set of peptides through the interaction between the peptide termini and conserved residues in MHC (2, 3). The peptides bound to a specific class I allotype share two or more relatively invariant residues (the anchor residues). The anchor residues bind in specific pockets generated by the polymorphic residues in the class I heavy chain (2, 4, 5). The peptide terminal residues and the anchor residues have a predictable orientation, whereas other residues in each peptide usually have unique main chain conformations and side chain orientations corresponding to their specific sequences (3). As yet, there is not a set of rules to predict the conformation of a peptide based on its sequence and the class I allotype to which it binds.

Recent crystallographic studies of TCR/class I complexes (A6/HLA-A2/Tax, B7/HLA-A2/Tax, 2C/H-2K^b/dEV8, and N15/H-2K^b/VSV8) (6–9) reveal a similar, diagonal orientation of the TCR over the peptide-binding cleft of each class I/peptide complex. The complementarity determining region (CDR) loops from each TCR (with the exception of CDR2β in A6 and CDR1β in B7) make contacts with both the peptide and the α1 and α2 helices of class I molecule, although the individual residues that are in contact with the CDRs are different in each class I. There are significant numbers of interactions between conserved class I residues and TCR, leading to the proposition that the orientation of TCR observed in these crystal structures is a general feature of most TCR/class I complexes. The conformation of the class I molecule remains the same both before and after TCR binding (6–9), although the center of the Tax peptide adjusts its conformation upon TCR binding in the A6/HLA-A2/Tax and B7/HLA-A2/Tax structures. Conversely, the peptide retains the same conformation in the 2C/H2-K^b/dEV8 structure (except for one side chain reorientation), but the CDR loops of the TCR (especially CDR1 and CDR3 in the α subunit) show

[1]*Abbreviations used in this paper:* β_2m, β_2-microglobulin; CDR, complementarity determining region.

large shifts relative to their positions in the structure of the uncomplexed 2C TCR. A similar comparison cannot be made for A6 and B7 because the unliganded structures are not known.

Although a TCR may often appear to be highly specific for a given cognate ligand, there are numerous examples in the literature of T cell cross-reactivity (10). Cross-recognized ligands can consist of different peptides presented by the same class I molecule, the same peptide presented by different class I allotypes, or distinct class I/peptide complexes. The ability of a single TCR to engage different but related ligands, either optimally or suboptimally, is proposed to play an important role in many immune processes (11–13).

Biochemical and molecular biological studies have been conducted to characterize the molecular basis for T cell cross-reactivity. The most popular model proposed from these studies is the molecular mimicry model, where different class I/peptide complexes form similar (spatially equivalent) antigenic surfaces in shape, charge, or both (14, 15). A recent paper (16) suggests a modified molecular mimicry model, in which a critical local charge mimicry formed by two residues contribute to the recognition of syngeneic and allogeneic class I/peptide complexes by the same TCR.

Cross-reactivity of TCR for different MHC allotypes within the same species is termed allo-reactivity, and cross-reactivity for MHC across species is termed xeno-reactivity. Xeno-reactivity requires the pairing of incompatible class I and CD8 molecules as well as the participation of incompatible costimulatory molecules for activation, and as such is more complicated than allo-reactivity. However, at the level of TCR and class I/peptide binding, xeno-reactivity can be viewed as an extreme case of T cell allo- or cross-reactivity. The study of a xeno-reactive system may reveal a more general mechanism which covers the whole scope of T cell cross-reactivity.

The $CD8^+$ CTL clone AHIII12.2 was derived from a C57BL/6 (H-2b) mouse injected with the human lymphoblastoid cell line JY (17). It engages in peptide-specific xeno-recognition of the human class I molecule HLA-A*0201 (designated A2) complexed with the peptide ALWGFFPVL (designated p1049). AHIII12.2 also recognizes murine class I H-$2D^b$ (designated D^b) complexed with the synthetic peptide FAPGFFPYL (designated p1058) and closely related analogues (18). The sequences of both the peptides and class I molecules are significantly different between these two complexes. Nevertheless, they are both recognized by a single TCR. Experiments done using singly substituted peptides indicate that the TCR cross-recognition of these ligands cannot be explained simply by a common motif defined at the level of the peptide (18).

Mutagenesis studies, although powerful, sometimes are difficult to interpret and are unable to provide a complete picture of the biological events involved. Therefore, we have engaged in the present study, and have determined the crystal structures of A2/p1049 and D^b complexed with p1027 (FAPGVFPYM) to 2.5 Å and 2.8 Å resolution, respectively. p1027 is a disubstituted analogue of p1058 and is an equally good agonist towards AHIII12.2 (data not shown). We chose p1027 rather than p1058 for the crystallographic study to maximize the primary sequence differences between the two class I/peptide complexes so that we can examine the extreme scope of T cell cross-reactivity. D^b/p1027 describes crystallographically how class I binds a peptide containing a noncanonical residue at an anchor position. More importantly, this study reveals, at a near atomic resolution, the molecular surfaces of two class I/peptide complexes recognized by the same TCR. A comparison of the potential TCR contacting surfaces shows that these two complexes do not possess obvious similarity. We propose that TCR binds the same areas of each class I molecule, utilizing both common and different contact residues in these areas. It requires that these contacts, although not identical between the two complexes, generate sufficient binding affinity between TCR and these complexes to allow for further T cell activation. This, rather than a simple common surface, accounts for the recognition of these two complexes by the same TCR.

Materials and Methods

Preparation of A2/p1049 and D^b/p1027. The cDNAs for D^b and murine β_2m were gifts from Dr. Stanley G. Nathenson (Albert Einstein College of Medicine, New York, NY) (19). A new construct of D^b was created to make it consistent with the length of the A2 construct (20). The new construct was generated by PCR amplifying residues 1–275 and was cloned into plasmid vector PLM1 (gifts from Dr. G. Verdine at Harvard University, Cambridge, MA). The protein was expressed in BL21pLysS cells (Invitrogen Corp.). Due to incorrect primer design, the first Gly residue of the heavy chain was left out, and three extra residues (ArgTrpGlu) were added to the COOH terminus of the heavy chain. The constructs of A2 heavy chain and human β_2m were identical to those described in Garboczi (20). Large quantities of A2, D^b, human β_2m, and murine β_2m were produced as inclusion bodies and purified as described previously (20).

Synthetic Peptides. Peptides used for crystallization were synthesized by the Peptide Synthesis Facility at the University of North Carolina at Chapel Hill (Chapel Hill, NC) and the National Cancer Institute at NIH (Bethesda, MD). All peptides were purified by reversed-phase HPLC to >95% purity, and the identities were confirmed by laser-desorption mass spectroscopy.

Crystallization. A2/p1049 and D^b/p1027 were folded in vitro as described in Garboczi (20). The folded complexes were concentrated using an Amicon ultrafiltration cell and purified by HPLC gel filtration chromatography (Biosep-SEC-S2000; Phenomenex). These complexes were further purified on a FPLC mono Q column (Pharmacia Biotech). Both complexes were crystallized using the hanging–drop vapor–diffusion method. The reservoir solution for A2/p1049 contained 12–16% PEG6000 and 6% dioxane in 25 mM MES buffer, pH 6.5. The hanging drop for A2/p1049 was a 1:1 mixture of the reservoir solution and 10 mg/ml protein in 25 mM MES, pH 6.5. The reservoir solution for D^b/p1027 contained 25% PEG8000, 150 mM NaCl, 0.8 M Gly, and 6% DMSO in 25 mM MES buffer, pH 6.5. The hanging drop was a 1:1 mixture of the reservoir solution and the protein solution which contained 10 mg/ml protein and 0.8 M Gly in 25 mM MES buffer, pH 6.5. Microseeding was necessary for both complexes to obtain crystals suitable for crystallographic studies.

Data Collection and Processing. Crystals of A2/p1049 were stored in 25 mM MES, pH 6.5, containing 20% PEG6000. Crystals of D^b/p1027 were stored in 25 mM MES, pH 6.5, containing 30% PEG8000 and 0.8 M Gly. These crystals were transferred directly into their corresponding storage buffer plus 30% glycerol, and were immediately placed in the cryo stream (generated by the Oxford Cryo System, and the temperature was set at 100 K). The diffraction data were collected on Rigaku R-Axis IIC using Cu Kα radiation.

The diffraction data were processed using the programs Denzo and Scalepack (21). Data statistics are shown in Table I.

Table I. *Summary of Crystallographic Analysis*

Parameters	A2/p1049	D^b/p1027
Space group	P1	C2
Cell dimensions	a = 50.09 Å	a = 91.35 Å
	b = 62.89 Å	b = 109.19 Å
	c = 74.68 Å	c = 57.78 Å
	α = 81.98°	α = 90.00°
	β = 76.18°	β = 122.81°
	γ = 77.86°	γ = 90.00°
Molecules/asymmetric unit	2	1
Resolution (Å)	2.5	2.8
Number of crystals	1	1
R_{merge} (%)*	8.3 (17.6)§	9.1 (29.2)
I/σ	16.6 (6.5)	20.4 (5.9)
Unique reflections	29804	11820
Total observations	77499	62278
Completeness (%)	90.9 (70.8)	99.9 (100.0)
Refinement ($F > 0$)		
Resolution (Å)	30–2.5	30–2.8
R_{work} (%)‡ (No. of reflections)	25.5 (25716)	25.2 (11200)
R_{free} (%) (No. of reflections)	30.4 (1363)	31.9 (559)
No. of nonhydrogen protein atoms	6320	3147
No. of water	50	5
Average B factor	37.06	34.39
R.m.s. deviations from ideality		
Bonds (Å)	0.007	0.007
Angles (°)	1.905	1.786
Dihedrals (°)	24.466	25.550
Impropers (°)	1.105	1.307
Residues in Ramanchandran plot (%)		
Most favored	90.1	89.3
Additional allowed	9.6	10.1
Generously allowed	0.3	0.6
Disallowed	0.0	0.0

*$R_{merge} = \Sigma_h\Sigma_i |I_{hi}-\langle I\rangle| / \Sigma_h\Sigma_i I_{hi}$, where I_{hi} is the observed intensity for each reflection h, and $\langle I\rangle$ is the average intensity of multiple observations of reflection h.

§Number in parentheses refers to the highest resolution shell (2.59–2.50 Å for A2/p1049 and 2.90–2.80 Å for D^b/p1027) unless otherwise stated.

‡$R = \Sigma_h ||F_{obs}| - k|F_{cal}|| / \Sigma_h |F_{obs}|$, where R_{free} is calculated for a randomly chosen 5% of reflections, R_{work} is calculated for the remaining 95% of reflections used for structure refinement.

Structure Determination. The structures of both complexes were determined using the Molecular Replacement method with the CCP4 program suite (22). The complex of HLA-A2 and a peptide from HIV reverse transcriptase (3) was used as a model for the structural solution for A2/p1049. H-2D^b complexed with a peptide (designated NP) from influenza virus (19) was used as the model for D^b/p1027. The orientation and position of these models were found using the program AMoRe in CCP4. Solvent flattening was applied to both crystals to improve the quality of the density. In addition, twofold averaging using the program DM in the CCP4 suite was applied to improve the density quality of A2/p1049. Manual model building into the electron density was performed using the program O (23).

Refinement of A2/p1049. Computational refinement was performed using the program X-PLOR version 3.851 (24) and Refmac in CCP4 (25). The structure was first refined in X-PLOR using 8–2.5 Å resolution data. Twofold noncrystallographic-symmetry restraints were applied to the two molecules in the asymmetric unit of HLA-A2/p1049 crystals with a weight of 300 kcal mol^{-1} $Å^{-2}$. Overall isotropic B factor refinement was performed first, then rigid body refinement was carried out using three domains: $\alpha1/\alpha2$, $\alpha3$, and β_2m. Overall anisotropic B factor refinement slightly improved R_{free} values. Cycles of computational refinement using positional refinement and simulated annealing (26) followed by manual model rebuilding using maps with coefficients 2fo-fc and fo-fc (after density modification using DM) were carried out. The X-PLOR refined structure was further refined using Refmac with strict noncrystallographic-symmetry restraints (see Refmac manual), a bulk solvent correction, overall anisotropic B factor correction, and individual B factor refinement. 50 water molecules were added in the structure using program ARP (27) in CCP4. The final R_{free} and R_{work} factors ($F > 0$) between 30 and 2.5 Å resolution are 30.4 and 25.5%, respectively. The refinement statistics are shown in Table I. The final real-space correlation coefficient (23) between the refined model and the DM-modified electron density map with coefficients 2fo-fc is 0.76. The conformation of the peptide was confirmed by the following averaged omit map procedure (Fig. 1 A). Masks including peptide were generated, but the peptide was omitted from the refined model to generate the phases for the initial map. Twofold averaging, solvent flattening, and histogram matching were applied with the program DM to generate the final omit map.

Refinement of D^b/p1027. D^b/p1027 was first refined in X-PLOR using 8.0–2.6 Å data. Rigid body refinement was performed similarly as in A2/p1049. Applying an overall anisotropic B factor was critical for the improvement of R_{free} and R_{work} factors. Simulated annealing was not helpful for improving the R_{free} in the case of D^b/p1027. Rounds of positional refinement and model rebuilding were carried out. The model rebuilding was largely based on the electron density maps using 2fo-fc and fo-fc coefficients. These maps were generated using 30–2.6 Å data although the refinement was only performed for 8–2.6 Å data. The peptide conformation and other suspicious residues were checked using omit maps. Omit maps were generated from simulated annealing procedures or by using the randomized omit map procedure described below. The X-PLOR refined structure was further refined by Refmac, as in A2/p1049. Individual B factor refinement significantly improved R_{free}. Thus individual B factor refinement was performed, although the number of parameters

refined was slightly over the number of reflections (Table I). After further consideration of the data quality, only data to 2.8 Å were used for the final round of refinement. The final R_{free} and R_{work} factors ($F > 0$) for D^b/p1027 between 30 and 2.8 Å are 31.9 and 25.2%, respectively. The refinement statistics are shown in Table I. The final real-space correlation coefficient (23) between the refined model and the solvent-flattened electron density map with coefficients 2fo-fc is 0.83.

All residues on the $\alpha1/\alpha2$ helices have clear and unambiguous densities. The peptide conformation was confirmed by a randomized omit map procedure (29) (Fig. 1 B). A random error <0.25 Å was added to each of the refined coordinates that did not contain peptide. These coordinates with the peptide region omitted were subject to Refmac refinement, and an omit electron density map with coefficients 2fo-fc was calculated. The omit map clearly indicates the side chain orientations, although the density is broken for the main chain between peptide residues 4 and 5, as well as between residues 5 and 6 (Fig. 1 B). Fig. 1 C shows the final 2fo-fc map surrounding the peptide. The only significant densities ($\sim3\sigma$ level) in the fo-fc map is a small positive peak near residue P5. This, in combination with the relatively weak main chain density near residue P5, may indicate some flexibility around the middle of the peptide.

The coordinates of both complexes have been deposited with the Protein Data Bank (Brookhaven, NY). Identifiers are 1b0g and 1bz9 for A2/p1049 and D^b/p1027, respectively.

Results and Discussion

Comparison of A2/p1049 and D^b/p1027 with Other Class I MHC/Peptide Complexes. Class I/peptide complexes have been extensively studied by crystallography. Detailed comparisons of class I/peptide structures have been presented elsewhere (1). Here we chose A2/RT (sequence ILKEPVHGV) (3) and D^b/NP (sequence ASNENMETM) (19) for comparison with A2/p1049 and D^b/p1027. These class I/peptide complexes have essentially identical backbone structures when individual domains (the $\alpha1/\alpha2$ superdomain, the $\alpha3$ domain, and β_2m) are superimposed. There is a relative domain movement of the $\alpha3$ domain and β_2m with respect to the $\alpha1/\alpha2$ superdomain when comparing D^b/p1027 with D^b/NP, as well as in comparing D^b/p1027 with A2/p1049 (Fig. 2 A). This type of domain movement has been observed in other class I crystal structures (2), and it could be an effect of the packing differences in the different crystal forms of these class I/peptide complexes.

When superimposing the $\alpha1/\alpha2$ superdomain (all peptides in this paper are compared by superimposing the $\alpha1/\alpha2$ superdomain), the ends of the peptide are essentially superimposable. However, the middle of the peptide (residues 3–7) has different backbone conformations and side chain orientations among these class I complexes (Fig. 2, B–D). This is consistent with earlier observations (3).

Peptide Binding in the Absence of a Canonical Anchor Residue. Sequence analysis of the peptides eluted from D^b complexes shows that D^b strongly prefers Asn at P5 and has a certain degree of preference for Met, Ile, or Leu at P9 (30). These observations are consistent with the D^b/NP crystal structure (19). Asn at P5 is deeply buried in a polar pocket defined by Glu^{A9}, Gln^{A70}, Gln^{A97}, and Tyr^{A156} (Fig. 3 A), and forms hydrogen bonds with the last three residues. (Throughout this paper, we use ^{A}, ^{B}, and ^{P} to represent class I heavy chain, β_2m, and peptide, respectively. Glu^{A9} refers to residue 9 of heavy chain, which is a Glu.) Met^{P9} is buried in a hydrophobic pocket formed by residues Phe^{A116}, Try^{A123}, Ile^{A124}, Thr^{A143}, and Trp^{A147}.

p1027 has the preferred anchor residue (Met) at P9, but it has Val rather than the normal anchor residue (Asn) at P5. The hydrophobic Val^{P5} of p1027 does not bind into

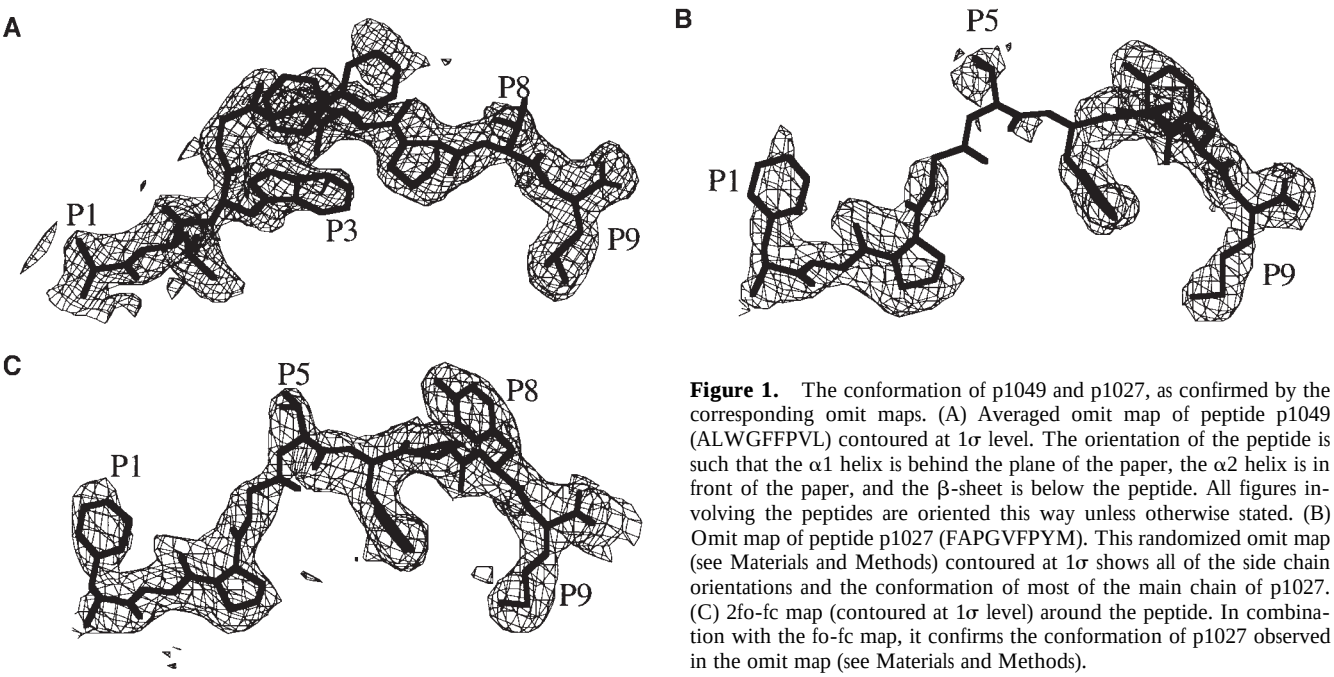

Figure 1. The conformation of p1049 and p1027, as confirmed by the corresponding omit maps. (A) Averaged omit map of peptide p1049 (ALWGFFPVL) contoured at 1σ level. The orientation of the peptide is such that the $\alpha1$ helix is behind the plane of the paper, the $\alpha2$ helix is in front of the paper, and the β-sheet is below the peptide. All figures involving the peptides are oriented this way unless otherwise stated. (B) Omit map of peptide p1027 (FAPGVFPYM). This randomized omit map (see Materials and Methods) contoured at 1σ shows all of the side chain orientations and the conformation of most of the main chain of p1027. (C) 2fo-fc map (contoured at 1σ level) around the peptide. In combination with the fo-fc map, it confirms the conformation of p1027 observed in the omit map (see Materials and Methods).

the highly polar pocket that accommodates Asn^{P5} of NP; it instead points up toward the solvent (Fig. 3 B). Phe^{P6} (the residue after Val^{P5}) inserts into the peptide binding cleft instead of pointing up as in the D^b/NP structure. Phe^{P6} would have clashed sterically with residue Tyr^{A156} if the tyrosine had remained in the same position as in D^b/NP. In D^b/p1027, the phenol ring of Tyr^{A156} swings away by roughly 55° to make space for Phe^{P6}. As a consequence, Phe^{P6} serves as a new adventitious anchor residue, and is buried in a hydrophobic pocket formed by residues Trp^{A73},

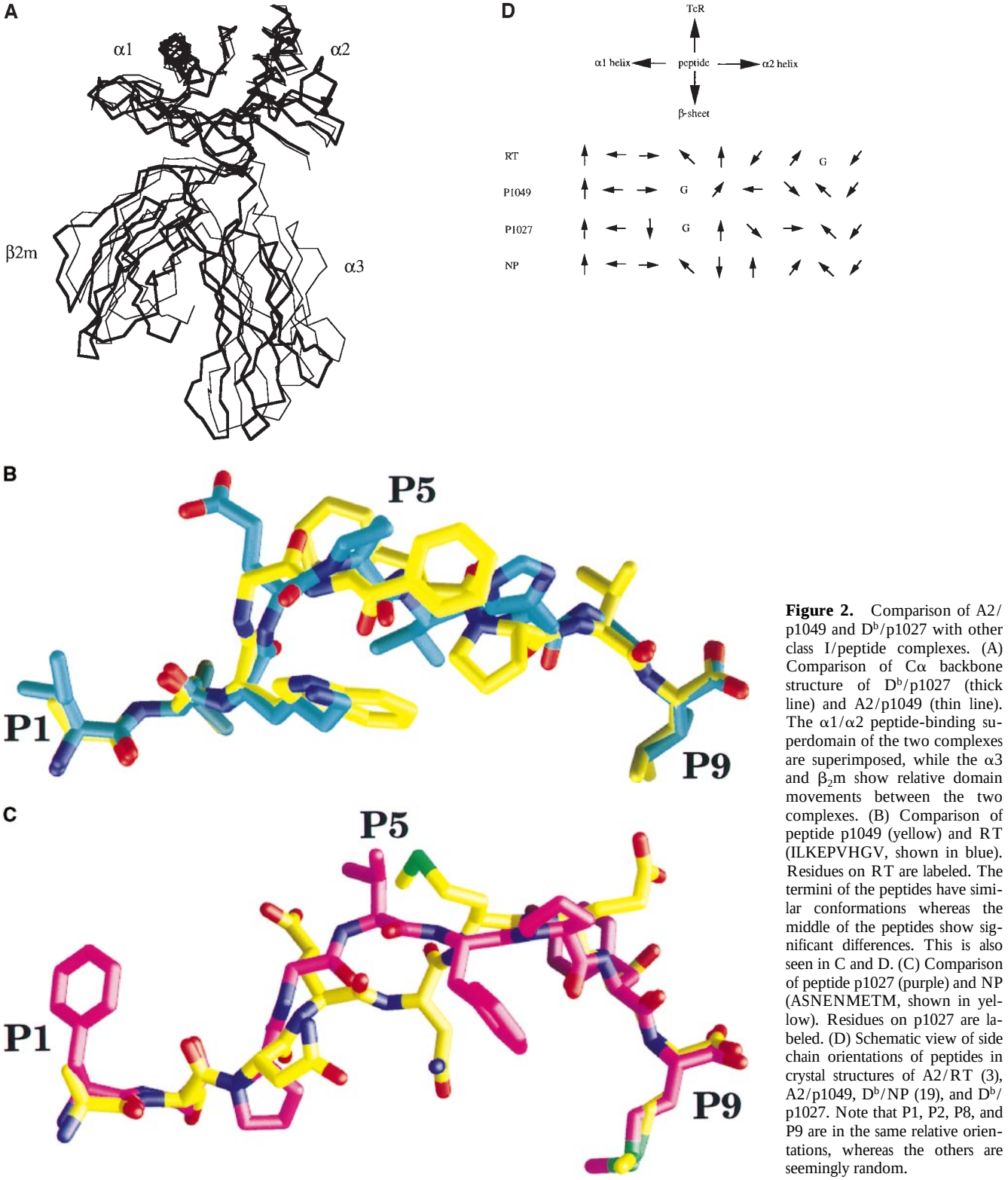

Figure 2. Comparison of A2/p1049 and D^b/p1027 with other class I/peptide complexes. (A) Comparison of Cα backbone structure of D^b/p1027 (thick line) and A2/p1049 (thin line). The α1/α2 peptide-binding superdomain of the two complexes are superimposed, while the α3 and β_2m show relative domain movements between the two complexes. (B) Comparison of peptide p1049 (yellow) and RT (ILKEPVHGV, shown in blue). Residues on RT are labeled. The termini of the peptides have similar conformations whereas the middle of the peptides show significant differences. This is also seen in C and D. (C) Comparison of peptide p1027 (purple) and NP (ASNENMETM, shown in yellow). Residues on p1027 are labeled. (D) Schematic view of side chain orientations of peptides in crystal structures of A2/RT (3), A2/p1049, D^b/NP (19), and D^b/p1027. Note that P1, P2, P8, and P9 are in the same relative orientations, whereas the others are seemingly random.

Leu^{A114}, Phe^{A116}, Trp^{A133}, Trp^{A147}, and the aromatic ring of Tyr^{A156} (Fig. 3 B). The original polar pocket changes its shape due to the movement of Tyr^{A156} (Fig. 3, A and B).

D^b/p1027 is the only crystal structure determined to date of a class I with a peptide that does not have the normal anchor residues. What we have observed in the structure of D^b/p1027 may be a general phenomenon. Other class I allotypes also occasionally bind peptides without primary anchor residues (31, 32). These peptides must also have compensated for the lost binding energy by using other residues within the peptide.

Comparison of TCR Contacting Regions in A2/p1049 and D^b/p1027. Several lines of evidence suggest that TCR docks on a common area and in a similar orientation on different class I/peptide complexes. In the four cocrystal structures of TCR/class I (6–9), the TCR is situated diagonally across the peptide-binding cleft with the TCR footprint centered on the peptide. The α subunit of TCR is located close to the NH_2 terminus of the peptide, while the β subunit is close to the COOH terminus of the peptide. Several contacts at the periphery of the TCR/class I interface involve conserved residues, which may help steer TCR into a general orientation. Recently, Smith and Lutz made exhaustive mutations on the α1 and α2 domains of class I molecule HLA-B7 and tested the recognition of these mutated molecules by 12 allospecific CTL clones. They concluded that the 12 CTL clones recognize a discrete surface with the bound peptide in the center. Although the boundaries of the TCR footprints from the 12 clones are not identical, they overlap largely.

Based on the crystal structure of A6/HLA-A2/Tax (6), the footprint of TCR can be approximated as a rectangular box with its width being ~22 Å, measured from the Cα atom of A65 to A157. The length of the rectangular box is ~32 Å, measured from the Cα atom of A170 to P9. The center of the rectangle is located near peptide residue P4. These dimensions are consistent with what is observed in the other TCR/MHC cocrystal structures (7, 8). It is also consistent with an earlier mutational study that suggests the TCR footprint is roughly 30 × 20 $Å^2$ (34). This rectangular box contains the peptide and the majority of the α1/α2 helices. In the following paragraphs, we first compare the peptide and the α1/α2 helices in A2/p1049 and D^b/p1027 at an atomic level. We then examine the shape and charge comparison of these two TCR footprints on the molecular surface diagrams.

The termini of p1027 and p1049 are fixed by a set of conserved hydrogen bonds and by specificity pockets that are complementary for the anchor residues, and thus they have similar conformations. The backbones of the first and last residues in p1049 and p1027 (Fig. 4 A) are essentially superimposable (rmsd 0.7 Å). The side chains of residues at the ends of the peptide (P1, P2, P8, and P9) have similar orientations. However, the average difference between Cα atoms of the middle residues (from P3 to P7) is 2.6 Å. The side chains of these middle residues also have different orientations (Fig. 4 A and Fig. 2 D). These differences result in different solvent accessibility patterns of the two peptides. In p1049, residue Phe^{P5} is the most solvent-exposed residue (Fig. 4 B). Residues in p1027 are more solvent accessible than those in p1049, as seen by the much higher protrusion formed by Val^{P5}. Residue Tyr^{P8} in p1027 is also significantly exposed to solvent (Fig. 4 B).

In the crystal structures of TCR complexed with A2/Tax (6) and K^b/dEV8 (8), 16 and 15 residues on their respective α1 and α2 helices were found to be in direct

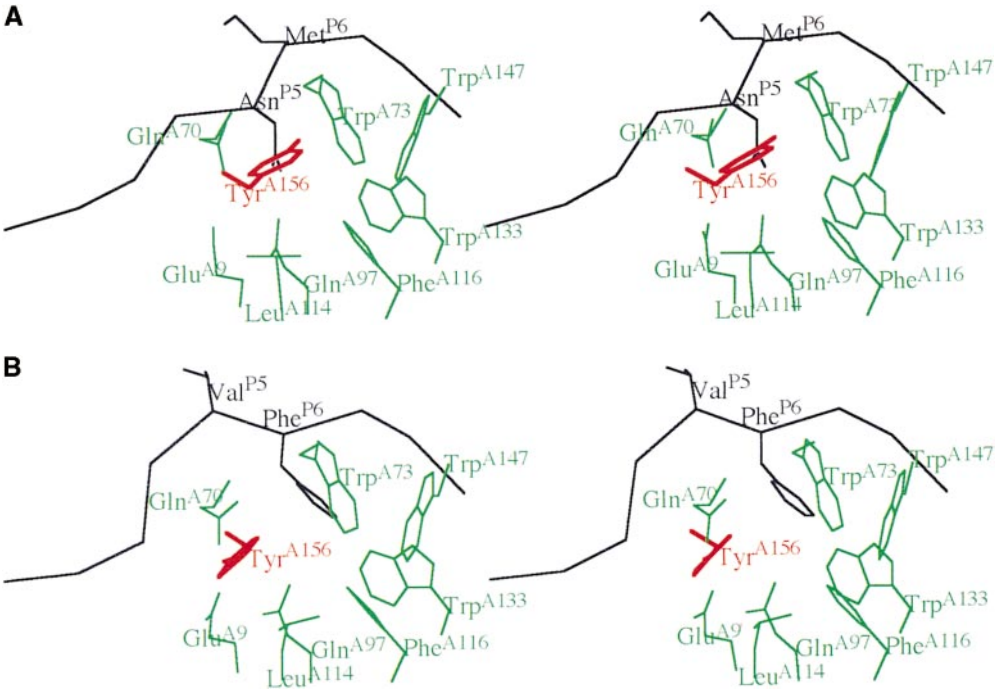

Figure 3. Anchor binding for D^b/p1027 compared to D^b/NP. (A) Stereo view of binding of anchor Asn^{P5} in D^b/NP. Peptide backbone is in black. D^b side chains in green. The Tyr that changes conformation during p1027 binding is shown in red. (B) Binding of adventitious anchor Phe^{P6} in D^b/p1027. Instead of the normal anchor residue Asn at P5, there is a Phe at P6 in p1027 that is used as an anchor. Color scheme is as in A.

contact with TCR. These TCR-contacting residues do not completely overlap between the two crystal structures. Since we cannot predict which set of residues will be utilized by D^b or A2 to interact with AHIII12.2, we will analyze all of these potential contacts. Based on the two cocrystal structures, there are 23 unique residues on A2/p1049 and D^b/p1027 that may interact with the AHIII12.2 TCR. Interestingly, these 23 residues include important residues for all TCR/class I/peptide complexes examined to date (7). 10 of these 23 residues are different between A2 and D^b (Table II and Fig. 5). Except for the conservative change from Ala to Gly at position A69, all the other changes involve dramatic charge, polarity, or size differences. Among the 13 residues with common amino-acid identities, some have taken different conformations between the two complexes (Fig. 5). Most of these common residues are highly conserved among different human or mouse class I alleles. For example, residue Lys^{A66} is conserved among 23 different HLA-A allotypes, and the remaining 12 residues are conserved among at least 49 different HLA-A allotypes. These conserved residues are likely to help dock the TCR in a common orientation on class I/peptide and contribute to the binding energy between TCR and class I/peptide. However, the different residues between these complexes also have to contribute significantly to the binding energy in order to differentiate between different antigenic complexes.

In Fig. 6, we placed the putative TCR footprint on the molecular surfaces of the crystal structures of A2/p1049 and D^b/p1027. Dispersed and local similarities exist between these two complexes, but there are many differences. The following is a comparison of the two structures from left to right with respect to Fig. 6.

In D^b/p1027, P1 is flanked by a pair of symmetrically located positive charges (Fig. 6 A), contributed on the left by Arg^{A62} and on the right by Lys^{A66} (Fig. 5 and Table II). In A2/p1049 A62 is a Gly instead of Arg, so there is no positive charge at the top left of P1 (Fig. 6 B). In A2/p1049, the positive patch on the right side of P1 is much larger than in D^b/p1027 because of the presence of Arg^{A65} in addition to Lys^{A66}. This additional positive charge does not exist in D^b/p1027, because in D^b residue A65 is a Gln. Due to the change of Arg^{A62} in D^b to Gly^{A62} in A2, residue Glu^{A63} is exposed and leads to the presence of a negative charge on the top of P1 in A2/p1049 not seen in D^b/p1027. However, the bottom left area of P1 is much more negatively charged in D^b/p1027 than the area in A2/p1049, due to the presence of Glu^{A163} in D^b, which is a Thr in A2.

P2 (Leu) in p1049 is buried in the HLA-A2 B pocket (35). P2 in p1027 points in the same direction, but is a much smaller residue (Ala). Neither makes any apparent contribution to the molecular surface in either structure. The position 3 residues (Trp in p1049 and Pro in p1027) are pointed into pocket D, away from the TCR contact

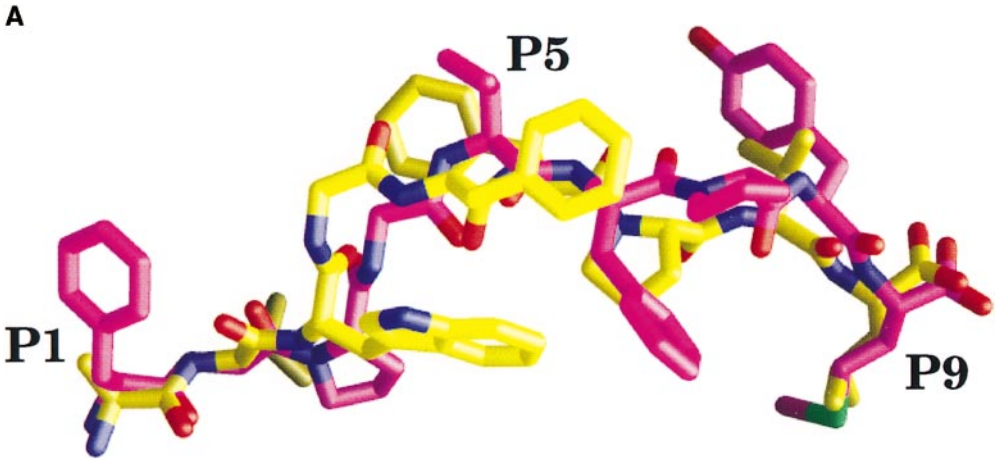

residue number	1	2	3	4	5	6	7	8	9
p1027	F	A	P	G	V	F	P	Y	M
solvent accessible surface (Å²)	25	2	1	33	146	20	38	93	0
p1049	A	L	W	G	F	F	P	V	L
solvent accessible surface (Å²)	0	3	13	41	83	53	3	49	1

Figure 4. Comparisons of the A2/p1049 and D^b/p1027 structures. (A) Comparison of peptide p1027 (FAPGVFPYM, shown in purple) and p1049 (ALWGFFPVL, shown in yellow). Residues on p1027 are labeled. Except for the first and last residues between the two peptides, the rest of the peptides are different. Note that residues in common between the two peptides (P6 and P7) are in different conformations. (B) Solvent accessibility of residues in p1027 (solid bars) and p1049 (striped bars). Percentage of solvent exposure is defined as the ratio of solvent accessible area in each residue to the total surface area of the corresponding amino acid. P5 is the most exposed residue in both peptides.

Table II. *Comparison of the 23 Residues on the α1/α2 Helices Proposed to Interact with TCR*

Residue number*	Amino acids in D^b/p1027	Amino acids in A2/p1049
58	Glu	Glu
62	**Arg**	**Gly**
65	**Gln**	**Arg**
66	Lys	Lys
68	Lys	Lys
69	**Gly**	**Ala**
72	Gln	Gln
73	**Trp**	**Thr**
76	Val	Val
79	**Arg**	**Gly**
146	Lys	Lys
149	**Gln**	**Ala**
150	**Ser**	**Ala**
151	**Gly**	**His**
154	Glu	Glu
155	**His**	**Gln**
158	Ala	Ala
159	Tyr	Tyr
162	Gly	Gly
163	**Glu**	**Thr**
166	Glu	Glu
167	Trp	Trp
170	Arg	Arg

*Residues that differ between the complexes are shown in bold.

surface. As can be seen in Fig. 3 C, these residues are almost completely buried and, similar to the P2 position, do not directly contribute to the molecular surface.

The next most prominent difference between the molecular surfaces is at the center of the peptide at P5. Peptide residue P5 protrudes higher in D^b/p1027 than in A2/p1049. The reason is obvious when comparing the orientations of P5 in p1027 and p1049 (Fig. 4 A and Fig. 2 D). Val^{P5} in p1027 points up, whereas Phe^{P5} in p1049 mainly points sideways. This is also consistent with the solvent accessibility of position P5 in the two peptides (Fig. 4, B and C). The OE1 atom of Glu^{A70} generates a negative charge above Val^{P5} in D^b/p1027, but there is no surface charge in A2 because residue 70 is a His and is buried underneath Phe^{P6}.

Positions 6 and 7 are identical in composition (Phe and Pro, respectively, for both A2/p1049 and D^b/p1027) but very different in orientation between the two complexes (Fig. 2 D and Fig. 4 A). Although both form hydrophobic patches, they constitute different topological surfaces to the right of the P5 protrusion. Position 8 is a Val in A2/p1049 and a Tyr in D^b/p1027. These residues are both solvent exposed (Fig. 4 B), but their differing size and chemical nature results in different surface properties in the P8 region of each complex.

There are similarities between the two molecular surfaces at the COOH end of the peptide along the right-hand border of the TCR footprint, generated by a common residue Lys^{A146}. This highly conserved Lys is located above and forms a salt bridge with the carboxylate of the peptide and covers the COOH terminus. A hydrophobic area surrounds this positive charge at Lys^{A146} in each complex. Close examination shows that the shapes of these hydrophobic areas are dissimilar. The depression observed beside the left edge of Lys^{A146} in Fig. 6 is much shallower in D^b/p1027 than in A2/p1049, due to three amino-acid changes. Residues Val^{P8}, Ala^{A150}, and Ala^{A149} in A2 are the much larger residues Tyr^{P8}, Ser^{A150}, and Gln^{A149} in D^b. Additionally, the orientation of Pro^{P7} is different between the two complexes and Pro^{P7} contributes to the shallow depression in D^b/p1027.

In summary, there appear to be few similarities in the TCR contact region of these two complexes when each area is examined in detail. There is similarity of gross fea-

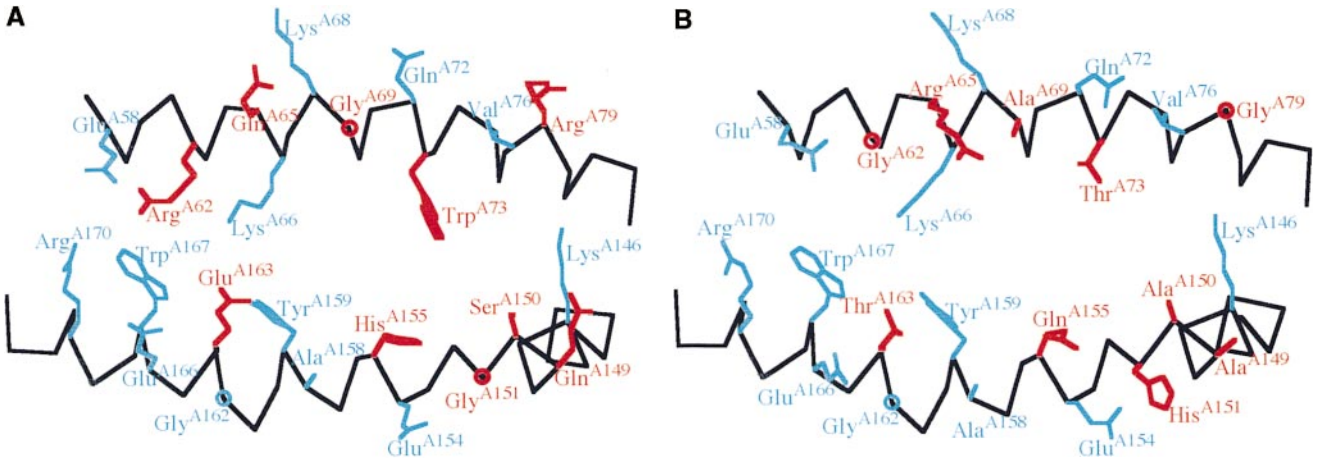

Figure 5. Comparison of residues on the α helices which potentially contact TCR in D^b/p1027 (A) and A2/p1049 (B). There are common residues (blue) between the two complexes, but significant differences (red) also exist.

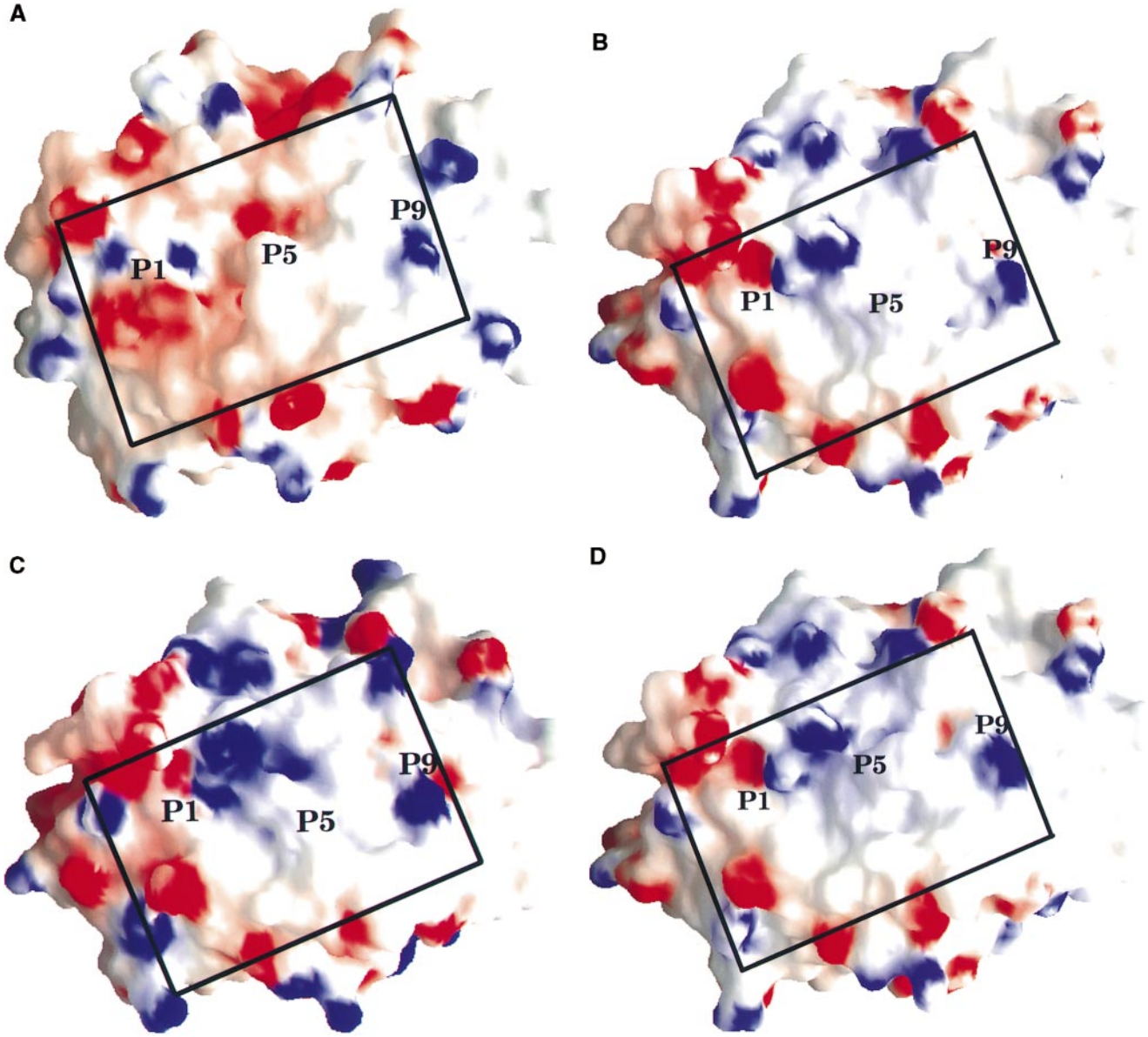

Figure 6. Comparison of molecular surfaces of A2/p1049 and D^b/p1027. (A) The molecular surface on the TCR contacting region of D^b/p1027 with the electrostatic potential mapped to the surface. This figure was generated using the program Grasp (45). Red and blue colors designate negative and positive charges, respectively. A, B, C, and D are top views of MHC/peptide complexes with the α1 helix on top of the diagram and the α2 helix on the bottom of the diagram. The rectangular box is a model TCR footprint derived from the crystal structure of A6/HLA-A2/Tax (6). (B) The molecular surface of A2/p1049. (C) The molecular surface of A2/matrix. (D) A speculative model of the molecular surface of A2/p1049 after the proposed conformational changes upon the engagement of the AHIII12.2 TCR. Comparison of A, B, and D shows that the TCR contacting surfaces in A2/p1049 and D^b/p1027 have similar features, but significant differences still exist. C indicates the existence of those similar features in a completely unrelated class I/peptide complex.

tures. The footprint is relatively acidic around P1, hydrophobic in the center, and basic around P9. However, these common features are largely formed by conserved residues in different class I allotypes. In A2/p1049, the acidic area around P1 is formed by residues Glu^{A58}, Glu^{A61}, and Glu^{A63}, and the positive charge around P9 is formed by residue Lys^{A146}. Residue A63 is conserved in 40 different HLA-A allotypes, and residues A58, A61, and A146 are conserved among 60 different HLA-A allotypes. The hydrophobic area in the center is largely formed by hydrophobic residues around peptide residue P5. Many peptides with hydrophobic residues at P5 and P6 do bind to A2 (30). Fig. 6 C shows the potential TCR contacting surface of a completely unrelated class I/peptide complex (A2/matrix peptide sequence GILGFVFTL) (3). It demonstrates that these common gross features exist on completely unrelated class I/peptide complexes. These features probably contribute to the binding of TCR in general and are most

likely the features that result in the similar orientation of TCR on MHC (7, 8). However, they cannot be the sole contributions, as they would lead to the recognition of many unrelated A2/peptide complexes by this TCR, which is obviously not the case.

Potential Conformational Changes of the Peptide. The A6/HLA-A2/Tax cocrystal structure shows that the Tax peptide changes conformation upon binding by TCR (6). Comparisons of the molecular surfaces of the A2/p1049 and D^b/p1027 complexes should also be evaluated with respect to potential conformational changes and to the new molecular surfaces that would be generated by such changes. Amino acid substitution experiments performed on A2/p1049 and D^b/p1058 can provide us with some information about the potential conformational changes of peptide upon TCR binding. The only differences between p1027 (FAPGVFPYM) and p1058 (FAPGFFPYL) are two conservative changes at P5 and P9. Leu is a preferred omega anchor residue for D^b bound peptides, but Met is a readily accepted substitute (30). The hydrophobic Phe^{P5} in p1058 is not likely to bind in the polar pocket normally designed for Asn^{P5}. It is more likely to be solvent exposed as is the Val in D^b/p1027. Thus, we believe that p1058 binds to D^b in a conformation roughly the same as p1027. The side chain orientations observed from the structure of D^b/p1027 are consistent with the TCR/MHC interaction data deduced from the amino acid substitution data generated previously (18). Therefore, it is likely that p1027 does not undergo any major conformational change upon TCR binding to D^b/p1027.

The Tax peptide changed conformation in both TCR/MHC cocrystal structures (6, 7). P6 moved away from the TCR and P7 moved toward the TCR. Residues P6 and P7 in p1049 may undergo similar conformational changes when engaging AHIII12.2. When Pro^{P7} is substituted with Ala, CTL reactivity is reduced to 40% of the wild-type level (18). Yet, in the crystal structure, Pro^{P7} points sideways toward the α2 helix and is solvent inaccessible. Thus, it is possible that Pro^{P7} changes conformation and points up and contacts the TCR upon binding. Accompanying the change on P7, P6 may move down as observed in Tax. If this is the case, it will generate a deeper depression surrounding P5 which will make the shape of the hydrophobic region surrounding residue P5 (Fig. 6, A and D) similar to that in D^b/p1027, but significant differences (especially charge distributions) would still exist between the footprints. Furthermore, although P8 in both peptides point up and are solvent accessible (Fig. 4, A and B), amino acid substitution experiments demonstrated that P8 in p1058 bound to D^b is in contact with TCR, while P8 in p1049 bound to A2 is not (18). These data confirm that the interactions between AHIII12.2 TCR and the two complexes are different.

Mechanism of T Cell Allo- and Xeno-recognition. The mechanism of T cell allo- and xeno-reactivity remains one of the paradoxes of modern immunology. Through positive and negative selection, T cells are educated in the thymus to recognize self-MHC complexed with foreign peptide in the periphery. The requirements for both MHC and peptide in selection are clear (36). However, even after thymic education, 1–10% of T cells still recognize allo- or xeno-MHC antigens that they could not have encountered before (14, 37). The most popular model proposed to answer this paradox is that the molecular surfaces of the allo- or xeno- and syngeneic MHC antigens are similar in shape or/and charge regardless of their derivation.

The comparison of the TCR contacting surfaces from the crystal structures shows that A2/p1049 and D^b/p1027 are different. These observations suggest that TCR cross-recognition of these class I/peptide epitopes is not due to simple shape and/or charge mimicry. Model building experiments on different allo- or cross-reactive class I have reached similar conclusions (38, 39). These observations, combined with the amino acid substitution data (18), can be best interpreted using a functional mimicry model, where TCR makes contacts with both common and different features on the two class I/peptide complexes and the mimicry is functional instead of structural. The common features between the two complexes mostly come from conserved residues and may help to steer TCR into a common orientation on different class I/peptide complexes. However, the noncommon features must also contribute significantly to ensure the specificity of a TCR.

When an allo- or xenogeneic class I interacts with a TCR, some of the residues under the TCR footprint remain the same as in the syngeneic complex, but other residues, perhaps many, will be different between these complexes. Among those changed residues, some will lose their interaction with TCR, but others will make adventitious contacts with TCR. Presumably, the lost and gained interactions will come to a balance, and the overall binding affinity between different class I ligands and TCR will be sufficient to trigger activation of the T cell. The relative importance of MHC versus peptide in this interaction is not predicted. There have been reports of peptide-independent TCR recognition of allo-reactive class I (40). This would suggest, for that case at least, that the contacts between the allo-reactive class I and TCR are sufficient to trigger the T cell, regardless of the peptide bound. Note also that this model does not suggest that either the TCR or class I has to be locked into a specific conformation. Loops and side chains of TCR may move to best accommodate the common and different contacts on a particular class I/peptide complex.

Recently, Speir et al. (16) generated a model of an allogeneic complex (L^d/QL9), based on the crystal structure of L^d with a mixture of peptides, and compared the model with the crystal structure of a syngeneic murine class I/peptide complex (K^b/dEV8). Based on these studies, they hypothesized a modified molecular mimicry model, in which a critical local charge mimicry (formed by residues Ser^{P7} and Asp^{A77} in K^b/dEV8 and Asp^{P8} and Asn^{A77} in L^d/QL9) contributes to the recognition of these two complexes by the same TCR. The functional mimicry model proposed here does not rule out the possibility of this modified molecular mimicry, but we think the original and modified molecular mimicry model does not account for all TCR cross-reactivity.

The cocrystal structures of A2/Tax with two different TCRs (A6 and B7) further demonstrate the requirement for flexibility in our thoughts about TCR recognition. A6 and B7 recognize A2/Tax by a common docking mechanism, but a different set of residues on the TCR is used to interact with A2/Tax. Only 1 of the 17 residues on the B7 TCR that contact A2/Tax is also found in the A6/A2/Tax interface. An additional 12 TCR residues that contact A2/Tax in the two TCRs are spatially equivalent, but they are different amino acids. Even when the TCR/MHC interactions were examined at an atomic level, few involved spatially equivalent and identical atoms. Most TCR/MHC interactions are between atomic pairs which are not spatially equivalent and/or have very different chemical natures. The sum of these common and different interactions must have generated sufficient affinity for the same class I to bind two different TCRs. It is not difficult to imagine that similar situations can happen between two different class I/peptide complexes with the same TCR.

Crystal structures of several antibody idiotope/antiidiotope complexes (41, 42) also demonstrate the absence of molecular mimicry between the antiidiotope and the antigen. Fields et al. (42) suggested that "the mimicking is functional, involving similar binding interactions, rather than exact topological replicas." For example, 6 out of the 12 hydrogen bonds are structurally (spatially) equivalent, although residues involved in these hydrogen bonds are amino acids with different size and chemical natures. We speculate that in many cases these interactions do not have to be structurally (or spatially) equivalent (as demonstrated by the cocrystal structure of TCRs A6 and B7 with A2/Tax); however, sufficient binding energy between antibody or TCR with its cross-reactive ligands can still be generated.

The functional mimicry model implies that TCR cross-reactivity, like antibody cross-reactivity, is unpredictable. It is possible for cross-reactive ligands to be structurally dissimilar, yet functionally similar. This mechanism also explains why the TCR repertoire selected by a single peptide can still recognize dissimilar ligands (43, 44). The different ligands are functionally similar with respect to recognition by the TCR.

We thank Drs. J. Frelinger, B. Wang, M. Batalia, and T. Kirksey for a critical reading of this manuscript. Also, we thank Shuqin Yan and Brian Cox for excellent technical assistance. We thank members of the Collins and Frelinger labs for stimulating discussions. Figures 1, 2 A, 3, and 5 were prepared using the program Molview written by Dr. Tom Smith at Purdue University.

R. Zhao is supported by a postdoctoral fellowship from the Cancer Research Institute. E.J. Collins acknowledges the support from National Institutes of Health grants AI29324 and AI20288.

Address correspondence to Edward J. Collins, Dept. of Microbiology and Immunology, CB#7290, 804 M.E. Jones Bldg., University of North Carolina at Chapel Hill, NC 27599. Phone: 919-966-6869; Fax: 919-962-8103; E-mail: collins1@med.unc.edu

Received for publication 29 July 1998 and in revised form 4 November 1998.

References

1. Batalia, M.A., and E.J. Collins. 1997. Peptide binding by class I and class II MHC molecules. *Biopolymers*. 43:281–302.
2. Fremont, D.H., M. Matsumura, E.A. Stura, P.A. Peterson, and I.A. Wilson. 1992. Crystal structures of two viral peptides in complex with murine MHC class I H-2K^b. *Science*. 257:919–927.
3. Madden, D.R., D.N. Garboczi, and D.C. Wiley. 1993. The antigenic identity of peptide–MHC complexes: a comparison of the conformations of five viral peptides presented by HLA-A2. *Cell*. 75:693–708.
4. Garrett, T.P.J., M.A. Saper, P.J. Bjorkman, J.L. Strominger, and D.C. Wiley. 1989. Specificity pockets for the side chains of peptide antigens in HLA-AW68. *Nature*. 341:692–696.
5. Guo, H.-C., T.S. Jardetzky, T.P.J. Garrett, W.S. Lane, J.L. Strominger, and D.C. Wiley. 1992. Different length polypeptides bind to HLA-Aw68 similarly at their ends but bulge out in the middle. *Nature*. 360:364–366.
6. Garboczi, D.N., P. Ghosh, U. Utz, W.R. Fan, W.E. Biddison, and D.C. Wiley. 1996. Structure of the complex between human T-cell receptor, viral peptide and HLA-A2. *Nature*. 384:134–141.
7. Ding, Y.-H., K.J. Smith, D.N. Garboczi, U. Utz, W.E. Biddison, and D.C. Wiley. 1998. Two human T cell receptors bind in a similar diagonal mode to the HLA-A2/Tax peptide complex using different TcR amino acids. *Immunity*. 8:403–411.
8. Garcia, K.C., M. Degano, L.R. Pease, M. Huang, P.A. Peterson, L. Teyton, and I.A. Wilson. 1998. Structural basis of plasticity in T cell receptor recognition of a self peptide–MHC antigen. *Science*. 279:1166–1172.
9. Teng, M.-K., A. Smolyar, A.G.D. Tse, J.-H. Liu, J. Liu, R.E. Hussey, S.G. Nathenson, H.-C. Chang, E.L. Reinherz, and J.-H. Wang. 1998. Identification of a common docking topology with substantial variation among different TcR–peptide–MHC complexes. *Curr. Biol*. 8:409–412.
10. Kersh, G.J., and P.M. Allen. 1996. Essential flexibility in the T-cell recognition of antigen. *Nature*. 380:495–498.
11. Grossman, Z., and A. Singer. 1996. Tuning of activation thresholds explains flexibility in the selection and development of T cells in the thymus. *Proc. Natl. Acad. Sci. USA*. 93: 14747–14752.
12. Oldstone, M.B.A. 1990. Molecular mimicry and autoim-

mune diseases. *Cell*. 50:819–820.
13. Theofilopolous, A.N. 1995. The basis of autoimmunity. I. Mechanisms of aberrant self-recognition. *Immunol. Today*. 16: 90–98.
14. Matzinger, P., and M.J. Bevan. 1977. Why do so many lymphocytes respond to major histocompatibility antigens? *Cell. Immunol*. 29:1–5.
15. Quaratino, S., C.J. Thorpe, P.J. Travers, and M. Londei. 1995. Similar antigenic surfaces, rather than sequence homology, dictate T-cell epitope molecular mimicry. *Proc. Natl. Acad. Sci. USA*. 92:10398–10402.
16. Speir, J.A., K.C. Garcia, A. Brunmark, M. Degano, P.A. Peterson, L. Teyton, and I. Wilson. 1998. Structural basis of 2C TcR allorecognition of H-2L^d peptide complexes. *Immunity*. 8:553–562.
17. Henderson, R.A., A.L. Cox, K. Sakaguchi, E. Appella, J. Shabanowitz, D.F. Junt, and V.H. Engelhard. 1993. Direct identification of an endogenous peptide recognized by multiple HLA-A2.1-specific cytotoxic T cells. *Proc. Natl. Acad. Sci. USA*. 90:10275–10279.
18. Loftus, D.J., Y. Chen, D.G. Covell, V.H. Engelhard, and E. Appella. 1997. Differential contact of disparate class I/peptide complexes as the basis for epitope cross-recognition by a single TCR. *J. Immunol*. 158:3651–3658.
19. Young, A.C.M., W. Zhang, J.C. Sacchettini, and S.G. Nathenson. 1994. The three-dimensional structure of H-2D^b at 2.4Å resolution: implications for antigen-determinant selection. *Cell*. 76:39–50.
20. Garboczi, D.N., D.T. Hung, and D.C. Wiley. 1992. HLA-A2–peptide complexes: refolding and crystallization of molecules expressed in *Escherichia coli* and complexed with single antigenic peptides. *Proc. Natl. Acad. Sci. USA*. 89:3429–3433.
21. Otwinowski, Z., and W. Minor. 1996. Processing of x-ray diffraction data collected in oscillation mode. *In* Methods in Enzymology. Vol. 276A. C.W.J. Carter and R.M. Sweet, editors. Academic Press, Inc., New York. 307–326.
22. Collaborative Computational Project Number 4. 1994. The CCP4 suite: programs for protein crystallography. *Acta Crystal. D*. 50:760–763.
23. Jones, T.A., J.-Y. Zou, S.W. Cowan, and M. Kjeldgaard. 1991. Improved methods for building protein models in electron density maps and the location of errors in these models. *Acta Crystal. A*. 47:110–119.
24. Brunger, A. 1992. X-PLOR (Version 3.1) A System for X-Ray Crystallography and NMR. Yale University Press, New Haven, CT. 382 pp.
25. Murshudov, G.N., A.A. Vagin, and E.J. Dodson. 1997. Refinement of macromolecular structures by the maximum-likelihood method. *Acta Crystal. D*. 53:240–255.
26. Brunger, A.T., A. Krukowski, and J. Erickson. 1990. Slow-cooling protocols for crystallographic refinement by simulated annealing. *Acta Crystal. A*. 46:585–593.
27. Lamzin, V.S., and K.S. Wilson. 1997. Automated refinement for protein crystallography. *In* Methods in Enzymology. Vol. 277B. C.W.J. Carter and R.M. Sweet, editors. Academic Press, Inc., New York. 269–305.
28. Brunger, A.T. 1992. The free R value: a novel statistical quantity for assessing the accuracy of crystal structures. *Nature*. 355:472–474.
29. McRee, D.E. 1993. Practical Protein Crystallography. Academic Press, Inc., San Diego, CA. 386 pp.
30. Falk, K., O. Rotzchke, S. Stevanovic, G. Jung, and H.-G. Rammensee. 1991. Allele-specific motifs revealed by sequencing of self-peptides eluted from MHC molecules. *Nature*. 351:290–296.
31. Mendoza, L.M., P. Paz, A. Zuberi, G. Christianson, D. Roopenian, and N. Shastri. 1997. Minors held by majors: the H13 minor histocompatibility locus defined as a peptide/MHC class I complex. *Immunity*. 7:461–472.
32. Burrows, G.G., K. Ariail, B. Celnik, J.E. Gambee, B.F.J. Bebo, H. Offner, and A.A. Vandenbark. 1996. Variation in H-2K(k) peptide motif revealed by sequencing naturally processed peptides from T-cell hybridoma class I molecules. *J. Neuro. Res*. 45:803–811.
33. Smith, K.D., and C.T. Lutz. 1997. Alloreactive T cell recognition of MHC class I molecules. *J. Immunol*. 158:2805–2812.
34. Ajitkumar, P., S.S. Geier, K.V. Kesari, F. Borriello, M. Nakagawa, J.A. Bluestone, M.A. Saper, D.C. Wiley, and S.G. Nathenson. 1988. Evidence that multiple residues on both the α-helices of the class I MHC molecule are simultaneously recognized by the T cell receptor. *Cell*. 54:47–56.
35. Saper, M.A., P.J. Bjorkman, and D.C. Wiley. 1991. Refined structure of the human histocompatibility antigen HLA-A2 at 2.6Å resolution. *J. Mol. Biol*. 219:277–319.
36. Benoist, C., and D. Mathis. 1997. Positive selection of T cells: fastidious or promiscuous? *Curr. Opin. Immunol*. 9:245–249.
37. Kaye, J., and C.A. Janeway, Jr. 1984. The Fab fragment of a directly activating monoclonal antibody that precipitates a disulfide-linked heterodimer from a helper T cell clone blocks activation by either allogeneic Ia or antigen and self-Ia. *J. Exp. Med*. 159:1397–1412.
38. Brock, R., K.-H. Wiesmuller, G. Jung, and P. Walden. 1996. Molecular basis for the recognition of two structurally different major histocompatibility complex/peptide complexes by a single T-cell receptor. *Proc. Natl. Acad. Sci. USA*. 93: 13108–13113.
39. Tallquist, M.D., A.J. Weaver, and L.R. Pease. 1998. Degenerate recognition of alloantigenic peptides on a positive-selecting class I molecule. *J. Immunol*. 160:802–809.
40. Smith, P.A., A. Brunmark, M.R. Jackson, and T.A. Potter. 1997. Peptide-independent recognition by alloreactive cytotoxic T lymphocytes (CTL). *J. Exp. Med*. 185:1023–1033.
41. Bentley, G.A., G. Boulot, M.M. Riottot, and R.J. Poljak. 1990. Three-dimensional structure of an idiotope–anti-idiotope complex. *Nature*. 348:254–257.
42. Fields, B.A., F.A. Goldbaum, X. Ysern, R.J. Poljak, and R.A. Mariuzza. 1995. Molecular basis of antigen mimicry by an anti-idiotope. *Nature*. 374:739–742.
43. Ignatowicz, L., J. Kappler, and P. Marrack. 1996. The repertoire of T cells shaped by a single MHC/peptide ligand. *Cell*. 84:521–529.
44. Liu, C.P., D. Parker, J. Kappler, and P. Marrack. 1997. Selection of antigen-specific T cells by a single IEk peptide combination. *J. Exp. Med*. 186:1441–1450.
45. Nichols, A., K.A. Sharp, and B. Honig. 1991. Protein folding and association: insights from the interfacial and thermodynamic properties of hydrocarbons. *Proteins*. 11:281–296.